Identification of Interdependencies and Prediction of Fault Propagation for Cyber-Physical Systems

Koosha Marashi[a], Sahra Sedigh Sarvestani[b,*], Ali R. Hurson[b]

[a]*Romeo Power Technology, Vernon, CA 90058, USA*
[b]*Missouri University of Science and Technology, Rolla, MO 65409, USA*

Abstract

Interdependence is an intrinsic feature of cyber-physical systems. Cyber and physical components are tightly integrated with each other, and hence, a trivial impairment in a part of the system may affect several components, leading to a sequence of failures that collapses the entire system. In this paper, we seek to identify the interdependencies among the components of a cyber-physical system using correlation metrics as well as a heuristic causation analysis method. We also demonstrate applicability of neural networks for prediction of imminent failures given the current system state. The proposed prediction tool can help system operators to perform timely preventive actions and mitigate the consequences of accidental failures and malicious attacks. As a case study, we have analyzed two smart grid test cases based on IEEE power bus systems, namely, IEEE–14 and IEEE–57.

Keywords: cyber-physical systems, interdependency, fault propagation, correlation and causation, failure prediction, neural networks, smart grid

1. Introduction

Complex systems exhibiting a tight coupling between physical processes and cyber infrastructures are known as cyber-physical systems (CPSs). Computational capabilities and communication technologies have enabled development of CPSs that can achieve higher dependability standards and provide

*Corresponding author

Email addresses: koosha@romeopower.com (Koosha Marashi), sedighs@mst.edu (Sahra Sedigh Sarvestani), hurson@mst.edu (Ali R. Hurson)

a better performance. The cyber infrastructure is the backbone of a CPS and provides wide-area measurement and monitoring, distributed control, and decision support.

The tight coupling of the physical and cyber networks are through links and various means of interactions, which makes them intertwined systems with intense interdependencies. *Interdependence* is a general term that accounts for a relationship among components of a system, where state of each component influences or is correlated with the state of others [1]. Interdependence can be categorized into different types and may exist at different levels, i.e., between systems, subsystems, or components. For example, a malfunctioning fuel pressure sensor in a car affecting its fuel economy manifests a functional interdependency in the engine subsystem. In an interdependent CPS, impairments originating in cyber and physical components may propagate through unprotected channels and escalate into a system-level failure. In general, interdependencies in a system can severely complicate the development of accurate models. This paper seeks to present a model of interdependency for CPSs, and develop a tool for predicting the components that are in risk of failure by reason of an earlier impairment.

There are numerous examples of large-scale systems being affected by impaired components or due to impairments in other correlated systems. The Arizona-Southern California blackout in September 2011, which occurred as a result of an 11-minute outage of a 500 kV transmission line is an example of cascading failures with profound consequences due to internal interdependencies within the boundaries of the Southwestern US power grid. The outage triggered a cascade that left approximately 2.7 million customers without power for up to 12 hours [2]. The Italy blackout, occurred in September 2003, is another example in which interdependencies among different infrastructures caused further outages [3]. This failure was exacerbated by the loss of Internet communication nodes left without power, which in turn caused further breakdown of communication and control at multiple power stations. Such incidents motivate our work on identification of cyber-physical interdependencies and prediction of imminent failures across the physical and cyber domains.

The need for proper preparation and planning has been emphasized in the task force reports of aforementioned and several other catastrophic events [2, 3, 4]. An interdependency model is the key in providing the knowledge needed for preparedness. In a disruption cycle of a system, interdependency models can substantially help at three stages:

Before disruption: Models can be developed to conduct simulations to improve awareness and understanding of the potential risks and their consequences, compare alternative recovery strategies, and enable contingency planning.

During disruption: Availability of knowledge and resources aid decision–making to mitigate consequences and support rapid recovery.

After disruption: Models can help in determining high-priority actions required for restoration of essential services as well as resources needed for supporting recovery. Models should be continually refined based on what was learned from the event.

There is an extensive literature devoted to the analysis of interdependency and its effects. In the area of critical infrastructure, Rinaldi et al. have provided an ontology for understanding interdependence and its classification into physical, cyber, geographic, and logical [1]. Researchers have used different approaches to identify interdependence among components, systems, or operations. In [5], the interdependencies between electrical infrastructure and the associated information infrastructure are qualitatively investigated and the pattern of fault propagation is explored. There are also examples of using correlation metrics for studying the interdependence. In [6], Pearson's correlation metric is used to investigate dependence among critical infrastructures after the World Trade Center attack. In another study [7], the time-series analysis method is utilized to reveal interdependencies across critical infrastructures from post-event restoration curves of February 2010 Chile earthquake.

Models of interdependency are presented using a variety of techniques such as topology-based and flow-based methods, Bayesian networks, and Petri nets. In [8], Beccuti et al. proposed an approach using stochastic Petri nets for modeling the operation of the physical and cyber networks in electric power delivery systems. They subsequently measured the effect of disruptions of one network on the other (e.g., as a result of a cyber attack) in terms of a number of domain-specific performance indices. The study presented in [9] utilizes graph-theoretic metrics to model cascading failures in power grids while the impacts of both load dynamics (physical domain) and node dependencies (cyber domain) are captured by applying topological constraints. In [10], a Markovian process model is used to encapsulate both stochastic and deterministic behaviors of a failure propagation scenario in

power systems. Although the cyber infrastructure is taken into account, the focus of authors is mainly on the application of multi-agent control techniques in the modern smart grids as well as their impacts and advantages on cascading failures. Another recent study presented in [11] attempts to improve interdependency models by accounting for the resilience of a given cyber or physical component against failures in its counterpart in the other network. This resilience is modeled using two-way probabilistic inter-network dependency joints.

Another group of studies are devoted to quantification of interdependencies. Casalicchio and Galli have presented a number of quantitative metrics for interdependencies in critical infrastructures and classified them into shape, core, and sector-specific metrics [12]. Studies presented in [13, 14] use topological metrics (e.g., connectivity and size of giant component) to quantify interdependency in a network; however, for the case of power grids, Verma et al. argue that topological measures that are not context-aware may underestimate vulnerability of the system [15].

As mentioned earlier, an important result of interdependency analysis is to predict the risk of failures for components and systems, prioritize preventive maintenance, and perform timely actions to mitigate effects of disruptions. In [16], statistical machine learning techniques were used to predict failure of feeder lines in boroughs of New York City over a three-month period and showed an acceptable accuracy of 75%. Additional results on application of the proposed methods are presented in [17]. In [18], authors use a graph-theoretical presentation of a power grid system that is coupled with a communication network. To model the propagation of failures in a cyber-physical power system, supervised machine learning techniques including polynomial and decision trees regression models are trained with synthetic failure data.

In this paper, our objective is to present a model of interdependency by observing sequence of failures for a set of failure cases and capturing the extent of interdependence with quantitative metrics as well as to provide a tool for prediction of failure sequences. We identify interdependencies among components of a CPS using correlation and causation analyses and quantify them with dependency metrics presented in our previous work [19]. Using the knowledge of the interdependency, we identify areas of the system where faults can propagate and create larger failures. We then create a set of failure cases and use the data from the resulting failure sequences to develop and configure an artificial neural network for prediction of fault propagation paths and cascading failures.

This work complements the study of Sturaro et al. in [18] by utilizing a domain-specific cyber-physical simulation tool to provide the resolution required for capturing behaviors of discrete-time cyber components in sensing, decision making, and control roles. The superiority of our method is that our simulation tool models the real-world physics of the underlying physical system, i.e., the interconnected electric delivery system and corresponding power components. The existing research on the use of machine learning tools and specifically neural network structures for prediction of networked systems largely relies on simplification of the physical attributes of the system to its topological specifications. The use of a domain-specific simulation tool strengthens our proposed method in two ways: i) validity of the synthesized failure data used for training and tunning of the prediction tool, and ii) correctness of the predictive performance evaluations. Our choice of simulation tool provides a high level of confidence in the overall validity of the proposed method as the outcomes are determined by the physical characteristics of the cyber and physical systems, not merely the topological configuration of the cyber-physical network. Our research paves the road to a better understanding of interdependencies in a system and prediction of its future failures. To illustrate our approach, we have applied it to two smart power grids based on the well-studied IEEE 14–bus and 57–bus test systems.

2. Interdependency Analysis

Dependency is a linkage between two entities, through which the state of one entity influences or is correlated with the state of the other. In this case, the relationship is usually unidirectional, i.e., entity i depends on j, but j does not depend on i. The influence of one entity on another can be exerted through intermediate entities, and need not be direct. In this paper, our focus is on functional dependencies between components of a single CPS. As an example, correct operation of a software that determines control commands for actuators in a robotic system is contingent on correct data from a sensor that detects surrounding objects. In this case, the software depends on the sensor, but the sensor does not depend on the software, as it can continue its operation regardless of the state of the software.

The terms "dependency" and "interdependency" are often used interchangeably. In this paper, our usage will be precise. We consider *interdependency* to describe *bidirectional* dependency, i.e., the state of an entity influences or is correlated with the state of another, and vice versa. In other

words, entity i depends on j through a number of links, and j likewise depends on i, possibly through different links. The interconnected topology and tight functional coupling typical of CPSs creates significant interdependency among components.

2.1. Representation of Interdependencies

For representation of interdependencies in a CPS, we use *dependency graph* that is a two-level weighted directed graph in which an edge exists from node i to node j if and only if the state of component i impacts, in one time step, the state of component j. Given a time step of sufficiently short duration, we can assume that impairment of a component propagates to the others through direct links only, not through multiple intermediate links.

Depending on the source and destination of an edge, it can represent one of four types of dependency, namely, physical-physical, physical-cyber, cyber-physical, and cyber-cyber. Note that in this notation, $s_1 - s_2$ represents a relation in which components of subsystem 1 (s_1) influence components of subsystem 2 (s_2). Figure 1 illustrates a dependency graph for a hypothetical CPS and specifies these four types of dependency. Note that in this context, "physical-cyber" and "cyber-physical" represent different types of dependencies. For example in the 2003 Italy blackout [3], the loss of telecommunication services that occurred following the initial power outage manifests a physical-cyber dependency, while the additional outages in the grid that took place because of the loss of control in the power stations indicates a cyber-physical dependency.

In Figure 1, the bottom plane encompasses components of the physical system and the top plane is representative of the cyber infrastructure that monitors and controls the underlying physical processes. The weights shown on the edges represent the extent of dependency, denoted as the *degree of influence* and are in the range of $[0, 1]$, where a 0 means that there is no functional influence from a component on another, and a 1 is the case where the state of a component causes maximal degradation to the state of another, i.e., makes it unable to operate.

For mathematical representation, we introduce a *direct influence matrix*, denoted as $\mathbf{D} = [d_{ij}] \in [0, 1]^{n \times n}$, which is in fact the adjacency matrix of the dependency graph. d_{ij} represents the *degree of influence* that component i exerts on component j and n is the total number of components in the system. Note that the entries on the diagonal of $\mathbf{D}$ should always equal zero,

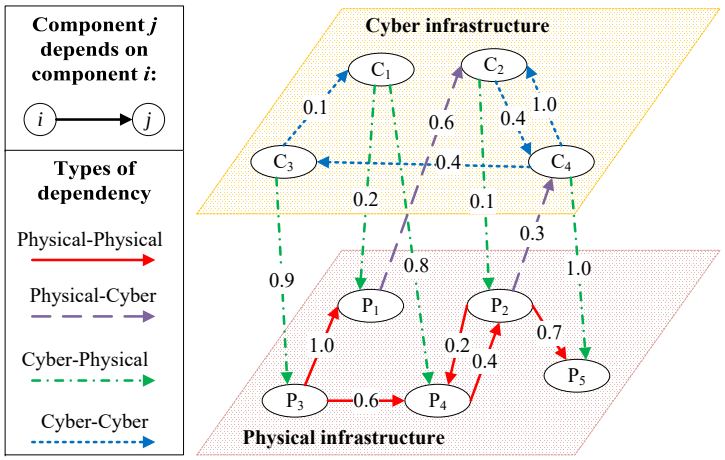

Figure 1: Dependency graph of a hypothetical CPS.

as a faulty state of a component "propagates" to itself immediately, not after one time step.

2.2. Identification of Interdependencies

Interdependency between components can be due to causality or simply correlation. In a causation relationship, the state of a component is responsible for that of another. On the other hand, the state of two components are correlated when they have a statistical relationship, whether causal or not. In a simple system with a processor that controls two actuators, it may be observed that the two actuators fail together, however, no cause-and-effect relationship is established. In fact, further analysis may reveal that the failure of the processor unit causes failure of both actuators, hence indicates simultaneity (a type of correlation) between failure of the two actuators without one being the actual reason for failure of the other. Depending on the purpose of interdependency analysis, either correlation or causation may be of interest. In this section, we present two approaches for analysis of causation and correlation, respectively, by observing sequence of failures for a set of failure cases.

A *failure case* describes a set of distinct components whose failure (assumed to be concurrent) initiates disturbance to the system. These initial disruptions, applied to the system at time $t = 0$, may propagate to other components through dependency links. For the disturbance initiated by failure case k, let $\mathcal{F}_k(t)$ represent the set of components that are observed to be

in a degraded state at time instant t. For failure case k, a *failure sequence* of length L represents L consecutive observations of the system state and is denoted as $\mathcal{F}_k(t), 0 \leq t < L$.

Our approach to identification of dependencies relies on observation of the system's behavior in response to each of a set of failure cases. The disruption associated with each failure case triggers a failure sequence, from which we infer dependency links between the components. The extent of dependency can be quantified with statistical methods such as correlation or causation analysis. The greater the number of failure cases, and the longer the duration of observation for each, the more accurate this inference will be. For collecting the failure sequences, it is possible to utilize data from simulation, laboratory and/or field observation, and/or historical data about failures of a system. In this paper, we present our results using data from a simulation environment.

2.2.1. Correlation Analysis

Correlation of two random variables reflects a statistical relationship, i.e., dependence between their values. A variety of existing measures can be used to quantify this dependence. For example, the Pearson correlation coefficient can capture linear dependence between two random variables. More sophisticated correlation measures can identify non-linear relationships as well and thus serve as powerful statistical tools for quantifying functional dependency between components.

For each component, we define a *state variable*, which is a random variable that characterizes the state of the component, then determine correlation between these random variables. Let $X_i(t)$ denote the state variable of component i at time t. For analysis of dependency of component j on component i, Pearson correlation coefficient (PCC) between $X_i(t)$ and $X_j(t)$ is calculated, as shown in Equation (1).

$$\rho_{X_i X_j} = \frac{\text{cov}(X_i, X_j)}{\sigma_{X_i} \sigma_{X_j}} \tag{1}$$

Where cov(.) is the covariance and σ is the standard deviation of a state variable. As noted in Section 2.1, we are interested in finding d_{ij} values, which represent dependence in one time step. Furthermore, direction of relationship (increasing or decreasing) is not of our interest. Therefore, we use $PCC_{X_i X_j} = |\rho_{X_i(t) X_j(t+1)}|$ to capture the direct dependency.

A shortcoming of PCC is that it only detects linear relationships, while an impaired component may result in disturbances in another component that are not necessarily linear. From various correlation coefficients introduced for detecting nonlinear relationships, we selected *randomized dependence coefficient* (RDC) [20], which has a low computational complexity and shows a good performance in comparison with similar methods. Readers are referred to [20] for more information on RDC. In this paper, we use $RDC_{X_iX_j}$ notation to represent RDC correlation between state variables X_i and X_j. Note that RDC has two parameters associated with it: sample size and number of random features, which are set following guidelines provided in [20].

For identification of interdependencies we can compute the mean value of correlation coefficients (either PCC or RDC) between X_i and X_j over all failure cases and use it as an estimator for d_{ij}.

2.2.2. Causation Analysis

In general, a causal relationship is harder to establish than correlation, and hence, fewer interdependency studies have investigated causality. We use a method inspired by the interaction model introduced in [21] to identify causation relationships and estimate $\mathbf{D}$. The work presented in [21] determines the interactions among components of a power grid, finds key dependency links, and provides strategies for mitigating cascading failures using a heuristic method. We present a similar method that is generalized to be applicable for cyber-physical systems. Specifically, we have extended the method to incorporate heterogeneous components, control the sensitivity in detecting causality, and account for dependency relationships between degraded states rather than binary states. We utilize a cyber-physical simulation environment and account for discrete-time behaviors of the cyber infrastructure, which is not possible in the OPA simulation environment employed in [21]. For validation of the basic proposed approach readers are referred to the original study [21].

Consider a system composed of n components, for which m failure cases are observed. Recall that for a given failure case k, the set $\mathcal{F}_k(t)$ is composed of all components that experienced degradation at time t. From the set of all failure sequences, i.e., $\mathcal{F}_k(t), \forall k$, we can construct the failure succession frequency matrix, $\mathbf{W} = [w_{ij}] \in \mathbb{Z}^{n\times n}$, where w_{ij} shows the number of times component j has degraded one time step after degradation of component i over all failure cases. Components in the set $\mathcal{F}_k(t-1)$ whose states are known to be the dominant causes for degradation of component j in $\mathcal{F}_k(t)$

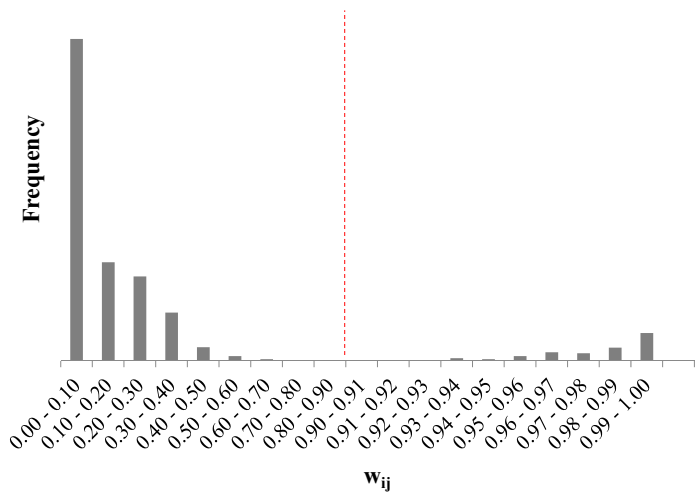

Figure 2: Histogram of w_{ij} among members of $\mathcal{F}_k$ in a representative system.

are identified using Equation (2).

$$\mathcal{H}_{k,j}(t) = \{\, i \mid i \in \mathcal{F}_k(t-1), w_{ij} \geq \alpha \max_{l \in \mathcal{F}_k(t-1)} w_{lj} \,\} \tag{2}$$

In Equation (2), α controls the threshold in detecting the causative relationships. Selection of α depends on the distribution of w_{ij} among the members of $\mathcal{F}_k$ set. In the histogram shown in Figure 2, we observe a significant separation between the members of $\mathcal{F}_k$ at about $w_{ij} = 0.9$, which allows us to easily distinguish correlative and causative relationships. For the systems studied in this work, the w_{ij} histograms follow a similar pattern to what is shown in Figure 2. Therefore, in all following analyses, we set α to 0.9 (shown as a red dotted line on Figure 2), i.e., $\mathcal{H}_{k,j}$ captures members of $\mathcal{F}_k$ whose w_{ij} value is larger than 0.9 (on the right of the red dotted line).

Matrix $\mathbf{E} = [e_{ij}] \in \mathbb{Z}^{n \times n}$ is constructed as shown in Equation (3), where e_{ij} is the number of times degradation of component i caused degradation of component j.

$$
\begin{aligned}
\mathbf{E} &= [e_{ij}] \\
e_{ij} &= \sum_{k=1}^{m} \sum_{t>0} \text{card}(\{\, (k,t) \mid i \in \mathcal{H}_{k,j}(t) \,\}) \qquad (3)
\end{aligned}
$$

In Equation (3), card(.) denotes the cardinality of a set. Assuming that N_i is the total number of times component i experiences degradation over all failure cases, $\frac{e_{ij}}{N_i}$ estimates the likelihood of component i having a causative relationship with component j. In other words, $\frac{e_{ij}}{N_i}$ represents the degree to which degradation of component i "causes" degradation in component j.

2.3. Quantification of Interdependencies

Assuming that the direct influence matrix $\mathbf{D}$ is known, we can explore dependency of components in multiple time steps. Specifically, we are interested in the kth*-level influence matrix*, which represents the influence that components have on each other over exactly k time steps – in contrast to $\mathbf{D}$, where the influence exerted over a single time step is captured. To this end, we first normalize $\mathbf{D}$ by dividing it by n to ensure that $\sum_{j=1}^{n} d_{ij} \leq 1$. Matrix $\left(\frac{1}{n}\mathbf{D}\right)^k$ is hence guaranteed to have an upper bound, and represents the kth-level influence matrix. The *total influence matrix*, $\mathbf{T}$, can be computed as shown in Equation (4).

$$
\begin{aligned}
\mathbf{T} &= [t_{ij}] = \mathbf{V} \circ \sum_{k=1}^{\infty} \left(\frac{1}{n}\mathbf{D}\right)^k \\
\mathbf{V} &= [v_{ij}] \\
v_{ij} &= \begin{cases} \dfrac{n+1}{n}, & i \neq j; \\ \dfrac{n+1}{n-1}, & i = j. \end{cases}, \quad 1 \leq i, j \leq n \qquad (4)
\end{aligned}
$$

In Equation (4), $\circ$ represents the entrywise product and t_{ij} shows the degree by which component j can be influenced by a failure in component i in any number of time steps, which reveals indirect influences. Note that the matrix $\mathbf{V}$ is used to scale t_{ij} to $[0, 1]$ range.

In Equations (5) and (6), we define τ_i, and ν_j, which are respectively the weighted out-degree of node i and weighted in-degree of node j, in order to evaluate the extent of influence components exert on or receive from other components.

$$\tau_i = \frac{1}{n}\sum_{j=1}^{n} t_{ij} \tag{5}$$

$$\nu_j = \frac{1}{n}\sum_{i=1}^{n} t_{ij} \tag{6}$$

We will also measure the average dependence that components of subsystem s_1 have on components of subsystem s_2. For this purpose, $\gamma_{s_1-s_2}$ is calculated as shown in Equation (7).

$$\gamma_{s_1-s_2} = \frac{1}{n_{s_1} n_{s_2}} \sum_{i\in s_1}\sum_{j\in s_2} t_{ij} \tag{7}$$

In Equation (7), n_{s_1} and n_{s_2} are the number of elements in subsystems s_1 and s_2, respectively, and $n_{s_1} + n_{s_2} = n$. Note that τ, ν, and $\gamma_{s_1-s_2}$ are all normalized to the $[0, 1]$ range so that systems of different sizes can be easily compared.

3. Prediction of Failure Sequences

Upon availability of knowledge of interdependency among the components of a system, a prediction tool may be used to detect catastrophic failures in their incipient stage and enable the supervisory control team to perform timely preventive actions and make appropriate decisions to mitigate the consequences [22, 23]. For this purpose, powerful and reliable tools are needed that are capable of identifying the components (or sections of the system) that are prone to failure as a result of a disruptive event. Furthermore, such tools are expected to respond in real-time and provide a prioritization of the components that are in risk, based on their failure likelihood and importance of their roles in the system.

The problem of predicting a sequence of events is closely related to classification and sequence labeling in time series analysis. In this work, we transform the problem of sequence prediction into a multi-class classification

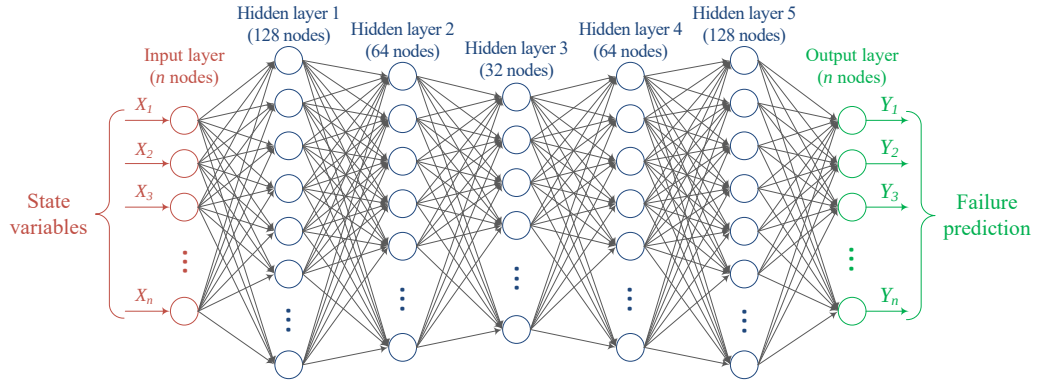

Figure 3: Architecture of the multi-layer fully connected ANN used for failure prediction.

and investigate the use of artificial neural networks (ANN) for tackling this problem. Reports show that ANNs are a promising tool for classification problems [24]. In a multi-class classification problem, a given instance is to be associated with a number of classes. The classification can also be probabilistic, where the classifier provides a probability distribution of a given instance belonging to the existing classes. Some of the popular classification problems are speech recognition, pattern recognition, and medical imaging.

For a system with n components, let $\mathbf{X}(t) = (X_1(t), X_2(t), \ldots, X_n(t))$ denote the input array to the ANN, where $X_i(t)$ is the state variable of component i at the time instance t. $\mathbf{X}(t)$ is fed to a multi-layer fully connected ANN with the architecture shown in Figure 3. The Output layer provides $\mathbf{Y} = (Y_1, Y_2, \ldots, Y_n)$, where Y_i represents the probability that component i fails as a result of the disruption specified by the given state variables in the input.

In the nodes of the hidden layers, we have used the softplus activation function [25], which is a differentiable and smooth version of the well-known rectifier function, to introduce nonlinearity to the ANN. The optimizer used for updating weights of the ANN is Adam, as introduced in [26], and the loss function is found by calculating the cross entropy between the sigmoid of the failure predictions and that of the actual failures. In order to prevent overfitting during the training process, we utilized the L_2 regularization method, which penalizes the network for large weights by increasing the loss.

The choice of ANN architecture is generally based on heuristic rules and is only for the sake of demonstrating applicability of the method. The choice

of number and size of the hidden layers is according to the previous studies on the performance of different ANNs in classification and time series prediction problems [27]. The bottleneck hidden layer structure used in this work is known to create a compressed representation of the information, and hence, acts as a nonlinear transformation and dimensionality reduction stage for the inputs. The number of hidden layers was selected through experimentation with available failure records and according to the quantitative performance metrics that are later discussed in 3.1. The number of nodes for each layer are chosen as powers of two to ensure computationally optimal matrix multiplications. Overall, the architecture presented here has shown an excellent performance on the test cases investigated in Section 4; however, depending on the type and size of the system under test, reconfiguration and adjustments may be necessary.

The ANN is trained using a dataset generated by simulating a number of failure cases or data from historical information of previous disruptions. In either case, each entry of the dataset should include the state variables of the components at the time of the disruptive event (input to the ANN), linked with the list of components affected consequently (used as ground truth for optimization during training and verification). In Section 4.4, we demonstrate the application of this ANN and provide its performance in predicting failures for two smart grid examples.

Depending on the type of the system, preventive actions may be prioritized based on different parameters. Examples of prioritization parameters are the predicted failure probability of each component (provided by the neural network), importance of each component in providing essential services, and consequences of failure of each component on other components (e.g., weighted out-degree, as defined in Section 2.3) as well as on the operation of the system (e.g., in terms of loss of dependability [28]).

3.1. Evaluation of Predictive Performance

In order to evaluate the effectiveness of the proposed ANN in predicting failures, we should use metrics that capture the predictive performance. To this end, we take advantage of the available metrics in the areas of information retrieval and classification, namely, accuracy, precision, recall, and F_1 score.

Accuracy is a measure of correct classification, but has shortcomings in capturing the performance when the number of failed components is small

compared to the total number of components, which is the case in our application. *Precision* shows the ratio of successful failure detections to total detections. Precision also has a shortcoming in evaluating the performance when the ANN correctly predicts only a portion of the failed components, but fails to detect the remainder. *Recall*, also known as sensitivity, is the ratio of the failed components detected by the ANN to the total number of failures. The shortcoming of recall is that its value is large if the ANN simply predicts that all of the components will fail. Therefore, no single metric is enough for evaluating the performance correctly. The F_1 *score* has been introduced to solve this issue by combining precision and recall into a single metric by taking their harmonic mean. Equation (8) shows how these metrics are calculated.

$$\begin{aligned} \text{Accuracy} &= \frac{tp + tn}{tp + tn + fp + fn} \\ \text{Precision} &= \frac{tp}{tp + fp} \\ \text{Recall} &= \frac{tp}{tp + fn} \\ F_1 \text{ score} &= 2 \times \frac{\text{Precision} \times \text{Recall}}{\text{Precision} + \text{Recall}} \end{aligned} \tag{8}$$

In Equation (8), tp, tn, fp, and fn represent the numbers of true positives, true negatives, false positives, and false negatives, respectively.

4. Case Study on Smart Grids

In this section, we demonstrate our proposed approach by applying it to two smart grids based on test systems well-studied in power engineering literature, namely, the IEEE 14– and IEEE 57–bus test systems [29]. The IEEE 14–bus system has been included in the interest of brevity and clarity and the IEEE 57–bus system demonstrates the scalability of our method. These systems are depicted in Figure 4.

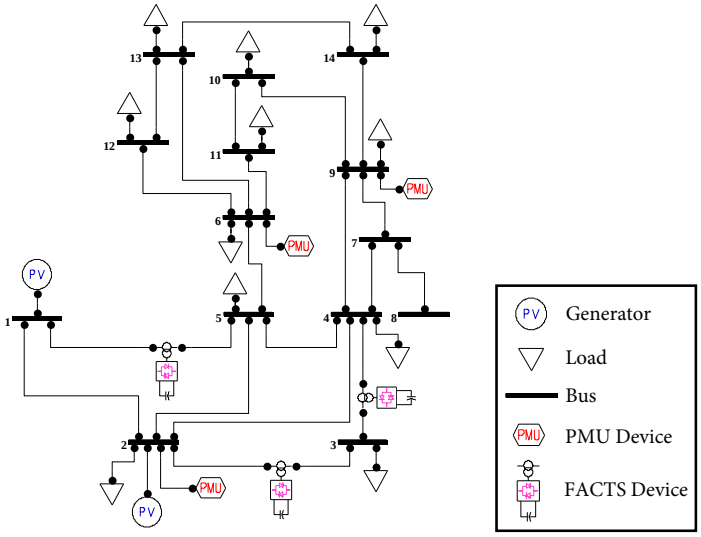

(a) IEEE 14–bus smart grid

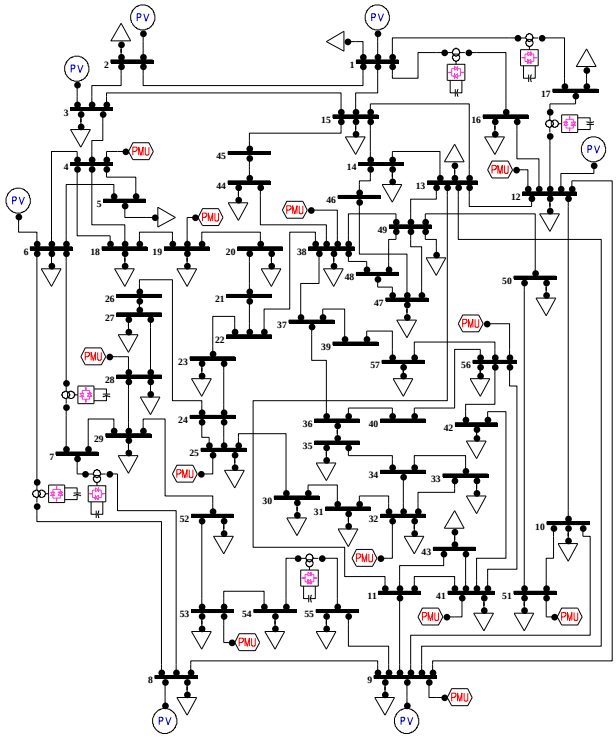

(b) IEEE 57–bus smart grid

Figure 4: Single line diagrams of IEEE smart grid test systems.

The classic IEEE test systems do not utilize any advanced cyber technologies and are merely composed of generators, transmission lines, transformers, buses, and loads. Since our approach is intended to be applicable to cyber-physical systems, we supplemented the classic IEEE test systems with cyber infrastructure to create equivalent smart grid systems for demonstration purposes. The cyber infrastructure is comprised of phasor measurement units (PMU), which record and communicate GPS-synchronized dynamic power system data, flexible AC transmission system (FACTS) devices, which adjust the flow of power in the transmission lines, and a decision support algorithm that determines optimal settings for the FACTS devices based on data from the PMUs. We applied the methods presented in [30] and [31] to determine the locations of the PMUs and FACTS devices on each smart grid (shown in Figure 4). We used a single-layer perceptron (not to be confused with the other ANN used for failure prediction introduced in Section 3) trained with $N-1$ contingencies as the decision support algorithm. For a more detailed explanation of the utilized cyber control scheme, readers are referred to our previous work [32, 33]. In the remainder of this paper, we use the following notations for the aforementioned components:

- L_{i-j}: A transmission line connecting bus i to bus j
- F_{i-j}: A series FACTS device installed on line L_{i-j}
- P_i: A PMU installed at bus i
- DS: The decision support algorithm

In addition to the intrinsic functional dependencies between components of smart grids, we assumed that the operation of PMU devices depends on the underlying power grid, i.e., a PMU device is disabled as soon as a voltage violation occurs at the bus on which it is installed. Voltage violation is defined to be outside of 0.9 to 1.1 per-unit range, according to the EN-50160 standard [34]. Note that we consciously simplify this dependency (no backup power or fallback mechanism) as it allows us to better understand the consequences of the dependency of the cyber network on the physical system.

4.1. Selection of Failure Cases

Selecting failure cases and determining the minimum number of failure cases needed for obtaining all of the dependencies are of great importance

in the presented method. In general, the larger the number of failure cases is, the more accurate the model becomes; however, exhaustive examination of failure cases is infeasible for large systems. The study presented in [21] provides a method for selection of failure cases in analysis of power grids while a given accuracy is maintained. In this work, we analyzed the following scenarios:

- One or two simultaneous transmission line outages,
- at most one failed FACTS device,
- at most one failed PMU, and
- failure of the decision support algorithm.

It is worth mentioning that upon availability of simulation environments capable of modeling the communication infrastructure with high resolution, considering the effects of respective impairments will improve the quality of the model. Unless a sophisticated model for channel impairments is utilized, inclusion of communication failures simply adds redundant failure cases and complicates representation of the results without actually capturing the behavior of data transport mechanisms. Therefore in this work, we have aggregated the failures of each communication link with those of the cyber component that receives the respective data. For example, a corrupted data package transmitted to a FACTS device is captured as a FACTS failure. Incorporating the manifestations of communication impairments guarantees that the model, despite the simplification, maintains all cyber-physical interdependencies. For instance, influence of a faulty PMU data on the operation of the decision support algorithm and corresponding FACTS device represents cyber-cyber dependencies.

Table 1 lists the number of simulations carried out for each test case. The total number of simulations for each system is the product of the number of failure cases shown for each category of component. Note that in all of the failure cases at least one transmission line is tripped since it is observed that the system does not degrade otherwise, even in the presence of cyber faults; however, once one or more transmission lines has tripped, impairment of cyber components can exacerbate the situation and lead to further degradation.

Table 1: Number of simulated failure cases.

	IEEE–14	IEEE–57
transmission lines	$\sum_{k=1}^{2} \binom{20}{k} = 210$	$\sum_{k=1}^{2} \binom{80}{k} = 3,240$
FACTS devices	$\sum_{k=0}^{1} \binom{3}{k} = 4$	$\sum_{k=0}^{1} \binom{7}{k} = 8$
PMU devices	$\sum_{k=0}^{1} \binom{3}{k} = 4$	$\sum_{k=0}^{1} \binom{12}{k} = 13$
decision support	$\sum_{k=0}^{1} \binom{1}{k} = 2$	$\sum_{k=0}^{1} \binom{1}{k} = 2$
total number of simulated cases	**6,720**	**673,920**

In this study, failure cases were selected based on the failure rate of components. Transmission lines were selected because they have a relatively high rate of failure and are a major source of power outages [35]. Additionally, we selected FACTS and PMU devices and the decision support as representative cyber components because their failure can impact the state of the physical components. Including other components of the system can enhance the model and improve the accuracy of results.

4.2. Simulations

For the electric delivery system, there are a number of commercial and non-commercial computer simulation tools available. The PowerWorld Simulator [36] is a popular commercial tool for analysis of high voltage power systems. It supports common protection and control devices, provides an interactive environment and intuitive GUI, and is able to solve power flow equations for very large systems; however, PowerWorld does not provide the transparency needed for analysis of the sequence of failures. Several other commercial software packages, such as DIgSILENT [37], have the same shortcoming. Among the non-commercial packages, MATPOWER [38] and PSAT [39] are two MATLAB-based toolboxes for Windows machines. MATPOWER can solve load flow and optimal power flow problems in a command line interface. PSAT has a graphical interface and supports basic monitoring and protection devices and power regulators in addition to the capabilities of MATPOWER. In this work, we used PSAT for simulation of the two IEEE bus systems. For the purpose of our simulations, we enhanced PSAT in order to achieve the high resolution required for analysis of smart

grids [32, 33]. These enhancements include incorporating wide-area measurement capabilities by PMU devices, providing a platform for implementing a decision support algorithm, and integrating the power systems with communication technologies used in smart grid applications. This modified version of PSAT is interfaced with a MATLAB wrapper that acts as an adapter between libraries and orchestrates subroutine calls.

The simulation environment is used to determine power flows and voltages in the system during the failure cases. For each failure case, specific faults are injected to predetermined components of the system by disabling FACTS devices, PMU devices, and decision support as well as tripping transmission lines. At each time step, PSAT performs power flow analysis and determines active power flow on each line and voltage at each bus. Active power flow of the lines are compared to their capacity, and if any line is overloaded, it is considered failed and the topology is updated accordingly. Since the cyber-physical dependencies are incorporated in the data models and enforced by the simulation environment, the propagation of the injected faults takes place automatically. For example, when the decision support platform receives a faulty data from a malfunctioning PMU, it is likely to send incorrect commands to respective FACTS devices. The FACTS devices will in turn apply wrong compensations and decrease power transfer capability of the system. The resulting load imbalance can overload and trip transmission lines and cause further cyber and/or physical failures. The simulation continues this automatic propagation of faults until no further failures are detected.

4.3. Interdependencies of IEEE Bus Systems

In this section, we present interdependencies of IEEE–14 and IEEE–57 smart grids identified using both correlation and causation analyses. Correlation analysis requires state variable for each component to be defined. Equation (9) shows definition of state variables for each category of components in smart grids.

$$
\begin{aligned}
X_{L_{i-j}}(t) &= \left|\text{Active power flow of } L_{i-j} \text{ in p.u. at time } t\right| \\
X_{F_{i-j}}(t) &= \begin{cases} 1, & F_{i-j} \text{ is operational at time } t; \\ 0, & \text{otherwise.} \end{cases} \\
X_{P_i}(t) &= \begin{cases} 1, & P_i \text{ is operational at time } t; \\ 0, & \text{otherwise.} \end{cases} \\
X_{DS}(t) &= \frac{\text{Number of observable buses and lines}}{\text{Total number of buses and lines}}
\end{aligned} \tag{9}
$$

In Equation (9), $X_{L_{i-j}}(t) \in \mathbb{R}^+$, $X_{F_{i-j}}(t) \in \{0,1\}$, $X_{P_i}(t) \in \{0,1\}$, and $X_{DS}(t) \in [0,1]$. Note that $X_{DS}(t)$ is the portion of the power system that is observable to the decision support and is used as a measure since it well captures its operation and data dependency on PMU devices. Figure 5 shows how these state variables can capture the operation of a smart grid during a failure sequence. In Figure 5, state variables of components of IEEE–14 smart grid during a selected failure sequence are plotted on a single horizontal axis. Note that the state variables are shown for components that experience degradation only. Each row presents the state variable of a component. The rows are ordered according to the propagation of the faults, i.e., the two topmost rows correspond to the components whose failure initiates the failure case (L_{1-5} and P_2); the third and fourth rows represent state variable of the components that fail consequently (L_{1-2} and F_{1-5}); and so forth.

According to Figure 5, the correlation among the state variables is expected to be maximal for those which degrade with one time step difference. Table 2 shows values of PCC and RDC for pairs of components that degrade with one time step difference as shown in Figure 5. In calculation of RDC values, sample size and number of random features are set to 0.1 and 1, respectively.

Both correlation coefficients exhibit relatively large values for the component pairs that are expected to have dependence; however, RDC values of dependent components better stand out according to Table 2. This is mainly due to the fact that RDC captures nonlinear as well as linear correlations, unlike PCC, which only captures linear relationships and results in underestimating dependency between component pairs that are non-linearly correlated. Hereinafter, we utilize and present RDC values only, due to its superiority in capturing interdependence.

For each failure case, RDC values are calculated for all pairs of state

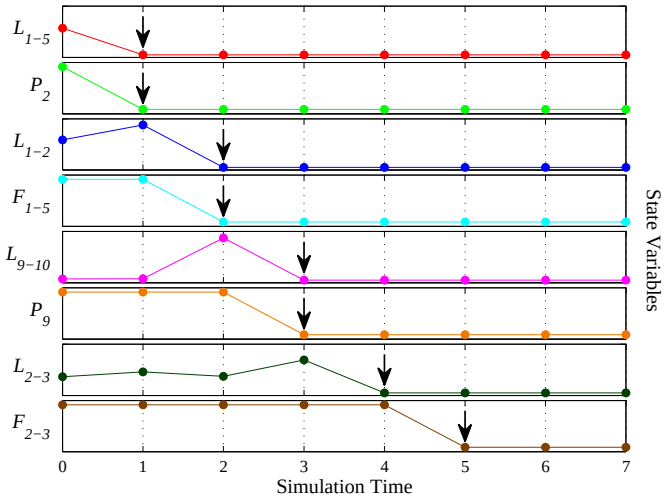

Figure 5: State variables of selected components of IEEE–14 during a failure sequence. Arrows indicate the points at which components are considered failed.

Table 2: Correlation coefficients between state variables of component pairs for those experience degradation with one time step difference in the failure case shown in Figure 5.

State variables		PCC	RDC
$X_{L_{1-5}}$	$X_{L_{1-2}}$	1.00	1.00
$X_{L_{1-5}}$	$X_{F_{1-5}}$	1.00	1.00
X_{P_2}	$X_{L_{1-2}}$	1.00	1.00
X_{P_2}	$X_{F_{1-5}}$	1.00	1.00
$X_{L_{1-2}}$	$X_{L_{9-10}}$	0.85	1.00
$X_{L_{1-2}}$	X_{P_9}	0.98	1.00
$X_{F_{1-5}}$	$X_{L_{9-10}}$	0.71	1.00
$X_{F_{1-5}}$	X_{P_9}	1.00	1.00
$X_{L_{9-10}}$	$X_{L_{2-3}}$	0.79	0.99
X_{P_9}	$X_{L_{2-3}}$	0.95	0.99
$X_{L_{2-3}}$	$X_{F_{2-3}}$	0.94	0.99
Maximum among all other pairs		0.68	0.83

variables. For estimating d_{ij} the mean value of $RDC_{X_i X_j}$ is calculated over all failure cases. Likewise, the process explained in Section 2.2.2 is applied on the results of simulations to find the d_{ij} values using causation analysis. For each of the methods, we found d_{ij} values and constructed the **D** matrix.

D matrices are visually represented as weighted directed graphs in Figure 6 and Figure 7 for IEEE–14 and IEEE–57 smart grid systems. Each edge represents a direct dependency and its width is proportional to the extent of the dependence (d_{ij}). Note that edges with weights less than 0.05 are not shown in the figures for ease of illustration. The top five links with largest weights are shown in red. It can be seen that dependency links with large weights are captured by both correlation and causation methods. It is also seen that the correlation-based method identifies a larger number of direct dependencies, as causation is typically a relationship that exists only in a small fraction of correlated events (also seen in Figure 2).

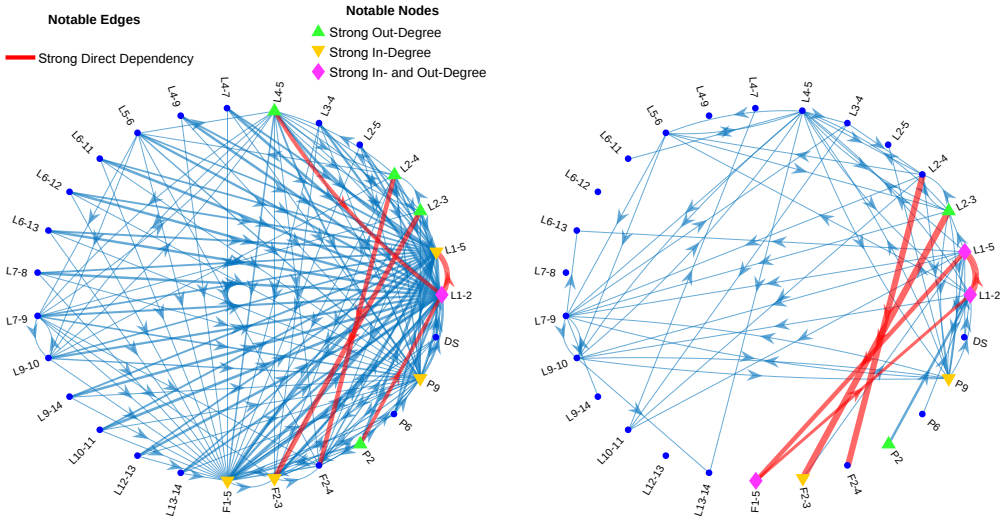

(a) Correlation (RDC)

(b) Causation

Figure 6: Graph representation of **D** matrix for IEEE–14 smart grid identified using correlation (a) and causation (b) analyses. Notable dependency links are shown in red.

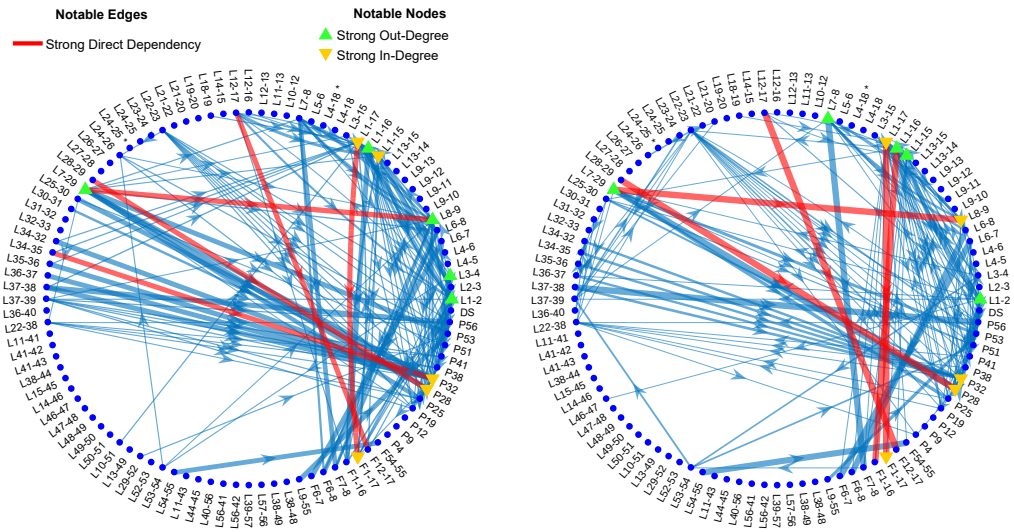

(a) Correlation (RDC) (b) Causation

Figure 7: Graph representation of **D** matrix for IEEE–57 smart grid identified using correlation (a) and causation (b) analyses. Notable dependency links are shown in red.

To verify correctness of the causation links identified, further analytical study is required. For the sake of brevity, we present our analysis on only the top five causation links shown in Figure 6b for IEEE-14. The most fragile section of the IEEE-14 system is the combination of L_{1-2} and L_{1-5}. In normal operation, the load on L_{1-5} is very small and the majority of the power is transmitted to the rest of the grid through L_{1-2}. In research studies on standard power test systems the capacity of each transmission line is usually assumed to be 120% or 125% of its power flow in normal operation. With this assumption, the capacity of L_{1-5} is significantly lower than that of L_{1-2}, and hence, upon tripping of L_{1-2}, the additional power flow that will have to be transmitted through L_{1-5} causes an overload. This confirms the causation link of $L_{1-2} - L_{1-5}$. In all cases of $L_{2-3} - F_{2-3}$, $L_{2-4} - F_{2-4}$, and $L_{1-5} - F_{1-5}$ a tripped transmission line causes its FACTS device to fail. These causation link are also valid as the FACTS devices are rendered inoperative upon outage of the respective transmission lines. Finally, the causation link of $F_{1-5} - L_{1-2}$ is valid as the only means of controlling the balance between L_{1-2} and L_{1-5} is through F_{1-5}, and hence, failure of F_{1-5} creates and imbalance that leads to an overload on L_{1-2}.

By applying interdependency quantification methods presented in Section

2.3, we computed the $\mathbf{T}$ matrix based on direct dependencies identified using both correlation and causation analyses. From the values of t_{ij} we can see links that are of great importance. As an example, in the IEEE–14 smart grid case, the total influence from the decision support to L_{1-5} is among the largest values while the corresponding direct link has a small weight of 0.05. The pair of P_{32} and F_{1-17} in the IEEE–57 smart grid is another example of a similar situation. This characteristic is justified by existence of several multi-step strong dependency links that connect pairs of components together and can give rise to further breakdown of components that are not in the geographical, logical, physical, or cyber reach of the initially impaired component [1]. This nonlocal property of the fault propagation has been observed in a number of real-world blackouts [3, 4].

In Figure 6 and Figure 7, the top five components (nodes) with highest in-degree (ν) and out-degree (τ) values are specified by distinguishable markers. This analysis identifies the cyber and physical elements that have the highest priority for further inspection and fortification if dependability is to be improved. Among the identified components are the bridge lines, which are responsible for transmitting the majority of the power from the generating buses to the load buses, as well as PMU and FACTS devices that are installed at critical locations of the power grid. Identifying these components using analytical methods can be very difficult or even impossible for large systems.

In order to compare the extent of dependency among the cyber and physical subsystems, $\gamma_{s_1-s_2}$ is calculated and shown in Figure 8.

It can be seen that the most significant dependencies are from the physical subsystem to the cyber subsystem (physical-cyber) and within the cyber subsystem (cyber-cyber). Dependency of cyber components on the physical components are typically in binary form (e.g., if power is not available the sensor shuts off) which justifies the large value of corresponding $\gamma_{s_1-s_2}$ value. The large value of cyber-cyber dependency is mainly due to the nature of the common topologies of the cyber infrastructure, in which each component is connected to multiple other components for transmission and reception of information.

Comparing the respective $\gamma_{s_1-s_2}$ values obtained from the correlation and causation analyses, we can infer that the causation relationships among the components are less frequent and of smaller extent, which can also be observed in the graphs provided in Figure 6 and Figure 7; however, the orders of $\gamma_{s_1-s_2}$ values within each group are similar to each other.

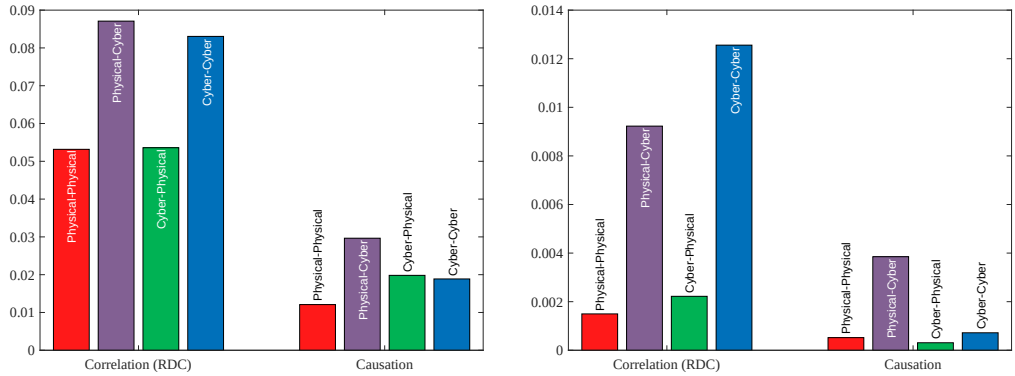

(a) IEEE–14 smart grid (b) IEEE–57 smart grid

Figure 8: Comparison of dependency among subsystems ($\gamma_{s_1-s_2}$) using correlation and causation analyses.

4.4. Prediction of Failures

For training the ANN, we need to convert the failure data into a dataset composed of several input/output elements. Figure 9 shows an example of a failure sequence for a hypothetical system with eight components. In this failure case, the system initially has faults in components 2 and 6. The faulty state is propagated to other components and affects component 1, then components 4 and 8, and finally component 5. We then transform this failure case into four entries of the dataset used for training the ANN, as shown in the right of Figure 9. Each entry of the dataset has two fields: i) an array of the state variables at a time instance and ii) a list of components that will degrade at the next time step.

The failure cases simulated for IEEE–14 and IEEE–57 smart grids resulted in datasets with several entries. Since the failure data for real-world large-scale CPSs is limited, we will investigate the possibility of training the ANN with a small subset of the available datasets and inspect its predictive capability. We randomly selected a subset of the available data and then divided them into training, validation, and test datasets using random selection. The training dataset is used for adjusting the weights of the ANN shown in Section 3 by backpropagation, while the validation dataset is employed as a recurrent feedback loop to minimize prediction error during the training cycles. This separation of training and validation datasets is done to prevent overfitting of the neural network. An overfitted model is one that

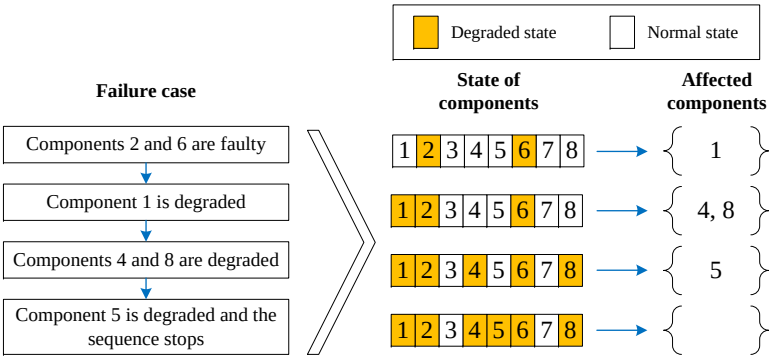

Figure 9: Transformation of a failure sequence into four entries of the dataset used for training the ANN.

Table 3: Size of the failure datasets used for the ANN.

Dataset	IEEE–14	IEEE–57
Total failure data available	17,968	1,181,871
Simple failure data used for the ANN	10,000	20,000
Training data (80%)	8,000	16,000
Validation data (10%)	1,000	2,000
Test data (10%)	1,000	2,000
Complex test data	1,000	1,000

corresponds very closely to the training dataset, and hence, may fail to make accurate predictions on future observations. Upon completion of the training, the test dataset is used for measuring the predictive performance of the ANN.

We also simulated a number of randomly selected more complex failure cases for each smart grid system and evaluated the performance of the ANN on predicting failures on those cases. The difference between the "simple" and the "complex" test data is that the latter is composed of failure cases with three to five concurrent transmission line failures, while the former is selected from the failure cases explained in Table 1, where at most two transmission lines are tripped concurrently. Table 3 shows the number of entries of the failure data used for the ANN.

Predictions on the failure cases from the complex datasets are expected to be harder for the ANN as they are not of the same type of the input data

Table 4: Predictive performance measures of the ANN.

System	Test Data	Precision	Recall	F_1 score
IEEE–14	Simple	99.25%	98.21%	98.46%
	Complex	90.63%	83.65%	85.54%
IEEE–57	Simple	99.38%	98.66%	98.87%
	Complex	84.83%	71.55%	75.29%

by which the ANN is trained. Performance measures of the ANN on simple and complex test datasets are shown in Table 4. It is worth mentioning that the failure prediction process, from inputting the system state to the ANN until receiving the output in the form of component indices that are about to fail, takes less than one millisecond on an Intel Xeon E5-2623 3.00 GHz machine. For implementation of the ANN, we used the TensorFlow package 1.2.0 [40] in Python 3.6.0.

As seen in Table 4, the ANN has an excellent performance on the simple datasets, both for IEEE–14 and IEEE–57 smart grids. Although the ANN does not perform as well on the complex datasets, its performance is still acceptable. The fact that the ANN can predict imminent failures with a high accuracy is mainly in virtue of the interdependence among the components and existence of recurred failure sequences. Identification of such sequences of failure that frequently occur is also useful in fortification of the system [28].

As mentioned earlier, we have performed the case study on a larger test system based on the IEEE–57 in order to evaluate the scalability of our approach. From Table 4, we can see that the ANN has a similar performance for IEEE–14 and IEEE-57 systems. Considering the fact that IEEE–14 is composed of 27 components (20 transmission lines, 3 FACTS devices, 3 PMU devices, and 1 decision support platform) while IEEE–57 has a total of 100 components (80 transmission lines, 7 FACTS devices, 12 PMU devices, and 1 decision support platform), the $100/27 \approx 3.7\times$ increase in the size of the system only requires a $2\times$ increase in the size of the training failure dataset from 8,000 to 16,000 (Table 3). This verifies the scalability of our prediction approach and its applicability to large-scale systems.

Thus far, we have seen that the ANN has a good performance in detecting the components that are about to fail, both with high accuracy and high speed. Another equally important feature of a prediction tool is that it maintains its performance when it is trained with a relatively small dataset.

In order to investigate whether the proposed approach has this feature and to find the minimum number of required entries in the training dataset, we have performed the training process with subsets of the available dataset and measured the predictive performance of the resulting ANN on a fixed test dataset. Figure 10 shows how the performance measures of the ANN in predicting failures of the IEEE–14 and IEEE–57 smart grids are affected by varying the size of the training dataset.

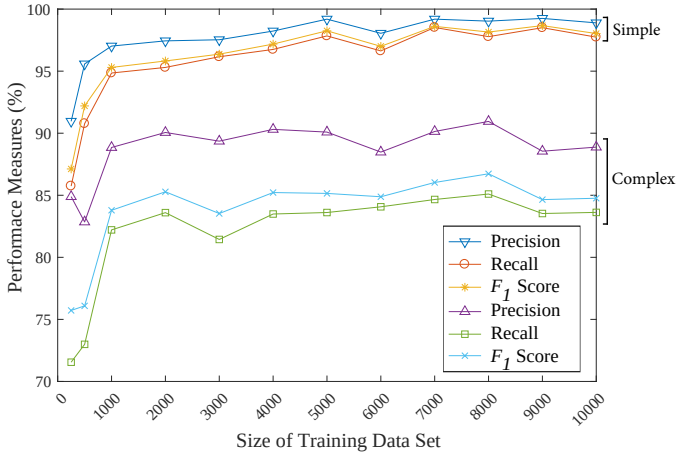

(a) IEEE–14 smart grid

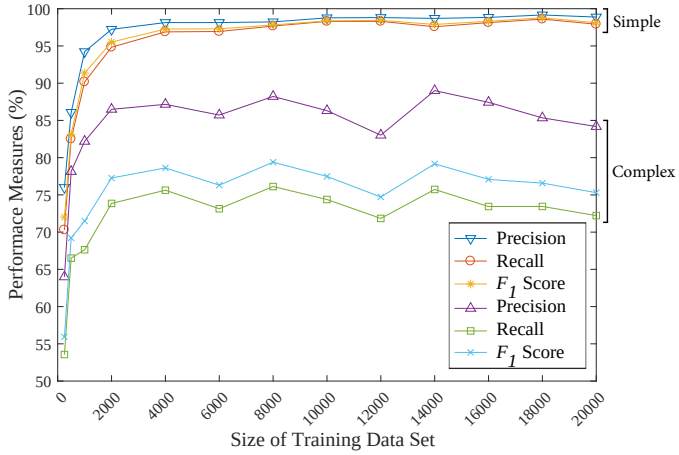

(b) IEEE–57 smart grid

Figure 10: The effect of the size of training dataset on predictive performance of the ANN.

As expected, it is seen in Figure 10 that the performance of the ANN

degrades as we decrease the size of the training dataset. Note that due to the randomness in selection of the training data, the performance curves are not monotonically increasing. According to Figure 10, increasing the size of the training dataset to more than 1000 for IEEE–14 smart grid and 2000 for IEEE–57 smart grid does not have a significant effect on the predictive performance of the ANN. Since the performance of the proposed ANN is not contingent on having large training datasets it can be trained using data available in the reports of the past power outages for developing a failure prediction tool for smart grids.

5. Conclusions

The research presented in this paper investigates the use of correlation and causation metrics for detection and quantification of the extent of dependency links among the components of a CPS. We provided the interdependency metrics, which seek to capture the effect of the multi-step dependencies as well as the immediate dependency links. These interdependency metrics revealed a number of dependency links among the components which were not in geographical, logical, physical, or cyber reach of each other. This nonlocal property of the fault propagation has been observed in the past and was shown on the test cases in this paper.

We also proposed a neural network approach for prediction of imminent component failures. Partly due to the high level of interdependence among the components of the analyzed systems, the neural network shows excellent predictive performance. This setup could detect the forthcoming failures with a high F_1 score of 98% on IEEE–14 and IEEE–57 smart grids. In the future of this research, we will take into account the effect of communication failures and consider more advanced ANN architectures in order to incorporate temporal features of the failures as well.

Acknowledgments

We gratefully acknowledge support from the US Departments of Education and Transportation for funding this project.

References

[1] S. Rinaldi, J. Peerenboom, T. Kelly, Identifying, understanding, and analyzing critical infrastructure interdependencies, IEEE Control Systems Magazine 11 (2001) 11–25.

[2] Federal Energy Regulatory Commission and North American Electric Reliability Corporation, Arizona-Southern California outages on September 8, 2011-causes and recommendations (April 2012).

[3] A. Berizzi, The Italian 2003 blackout, in: IEEE Power Eng. Soc. General Meeting, 2004, pp. 1673–1679.

[4] Final report on the August 14, 2003 blackout in the United States and Canada: Causes and recommendations, Tech. rep., U.S.-Canada Power System Outage Task Force (April 2004).

[5] J.-C. Laprie, K. Kanoun, M. Kaâniche, Modelling interdependencies between the electricity and information infrastructures, in: Proc. of the 26th Int. Conf. on Computer Safety, Rel. and Security (SAFECOMP), Vol. 4680, 2007, pp. 54–67. doi:10.1007/978-3-540-75101-4_5.

[6] D. Mendonça, W. A. Wallace, Impacts of the 2001 World Trade Center attack on New York City critical infrastructures, Journal of Infrastructure Systems 12 (4) (2006) 260–270. doi:10.1061/(ASCE)1076-0342(2006)12:4(260).

[7] L. Duenas-Osorio, A. Kwasinski, Quantification of lifeline system interdependencies after the 27 February 2010 Mw 8.8 offshore Maule, Chile, earthquake, Earthquake Spectra 28 (S1) (2012) S581–S603. doi:10.1193/1.4000054.

[8] M. Beccuti, S. Chiaradonna, F. D. Giandomenico, S. Donatelli, G. Dondossola, G. Franceschinis, Quantification of dependencies between electrical and information infrastructures, Int. Journal of Critical Infrastructure Protection 5 (1) (2012) 14 – 27. doi:10.1016/j.ijcip.2012.01.003.

[9] J. Zhou, N. Huang, D. W. Coit, F. A. Felder, Combined effects of load dynamics and dependence clusters on cascading failures in network systems, Rel. Eng. & Syst. Safety 170 (2018) 116 – 126. doi:10.1016/j.ress.2017.10.008.

[10] H. Guo, S. S. Yu, H. H. C. Iu, T. Fernando, C. Zheng, A complex network theory analytical approach to power system cascading failure–from a cyber-physical perspective, Chaos: An Interdisciplinary Journal of Nonlinear Science 29 (5) (2019) 053111. doi:10.1063/1.5092629.

[11] H. Tu, Y. Xia, J. Wu, X. Zhou, Robustness assessment of cyber–physical systems with weak interdependency, Physica A: Statistical Mechanics and its Applications 522 (2019) 9 – 17. doi:10.1016/j.physa.2019.01.137.

[12] E. Casalicchio, E. Galli, Metrics for quantifying interdependencies, in: Critical Infrastructure Protection II, Vol. 290, 2008, pp. 215–227. doi:10.1007/978-0-387-88523-0_16.

[13] Z. Huang, C. Wang, M. Stojmenovic, A. Nayak, Characterization of cascading failures in interdependent cyber-physical systems, IEEE Trans. Comput. 64 (8) (2015) 2158–2168. doi:10.1109/TC.2014.2360537.

[14] D. Zhou, J. Gao, H. E. Stanley, S. Havlin, Percolation of partially interdependent scale-free networks, Phys. Rev. E 87 (2013) 052812. doi:10.1103/PhysRevE.87.052812.

[15] T. Verma, W. Ellens, R. E. Kooij, Context-independent centrality measures underestimate the vulnerability of power grids, Int. Journal of Critical Infrastructures 11 (1) (2015) 62–81. doi:10.1504/IJCIS.2015.067398.

[16] P. Gross, A. Boulanger, M. Arias, D. Waltz, P. M. Long, C. Lawson, R. Anderson, M. Koenig, M. Mastrocinque, W. Fairechio, J. A. Johnson, S. Lee, F. Doherty, A. Kressner, Predicting electricity distribution feeder failures using machine learning susceptibility analysis, in: Proc. of the 18th Conf. on Innovative Applications of Artificial Intelligence, Vol. 2, 2006, pp. 1705–1711.

[17] C. Rudin, D. Waltz, R. N. Anderson, A. Boulanger, A. Salleb-Aouissi, M. Chow, H. Dutta, P. N. Gross, B. Huang, S. Ierome, D. F. Isaac, A. Kressner, R. J. Passonneau, A. Radeva, L. Wu, Machine learning for the New York City power grid, IEEE Trans. Pattern Anal. Mach. Intell. 34 (2) (2012) 328–345. doi:10.1109/TPAMI.2011.108.

[18] A. Sturaro, S. Silvestri, M. Conti, S. K. Das, A realistic model for failure propagation in interdependent cyber-physical systems, IEEE Trans. Netw. Sci. Eng. 7 (2) (2020) 817–831. doi:10.1109/TNSE.2018.2872034.

[19] K. Marashi, S. Sedigh Sarvestani, A. R. Hurson, Quantification and analysis of interdependency in cyber-physical systems, in: Proc. of the 3rd Int. Workshop on Reliability and Security Aspects for Critical Infrastructure (ReSA4CI 2016), in conjunction with the 46th IEEE/IFIP Int. Conf. on Dependable Systems and Networks (DSN 2016), Toulouse, France, 2016, pp. 149–154. doi:10.1109/DSN-W.2016.47.

[20] D. Lopez-Paz, P. Hennig, B. Schölkopf, The randomized dependence coefficient, in: Advances in Neural Information Processing Systems, 2013, pp. 1–9.

[21] J. Qi, K. Sun, S. Mei, An interaction model for simulation and mitigation of cascading failures, IEEE Trans. Power Syst. 30 (2) (2015) 804–819. doi:10.1109/TPWRS.2014.2337284.

[22] M. Afshari, A. Mahajan, Static teams with common information, IFAC-PapersOnLine 50 (1) (2017) 11926 – 11931. doi:10.1016/j.ifacol.2017.08.1449.

[23] M. Afshari, A. Mahajan, Team optimal decentralized state estimation, in: IEEE Conference on Decision and Control, 2018, pp. 5044–5050. doi:10.1109/CDC.2018.8619493.

[24] G. Ou, Y. L. Murphey, Multi-class pattern classification using neural networks, Pattern Recognition 40 (1) (2007) 4 – 18. doi:10.1016/j.patcog.2006.04.041.

[25] C. Dugas, Y. Bengio, F. Bélisle, C. Nadeau, R. Garcia, Incorporating second-order functional knowledge for better option pricing, in: Proc. of the 13th Int. Conf. on Neural Information Processing Systems, Cambridge, MA, USA, 2000, pp. 451–457.

[26] D. P. Kingma, J. Ba, Adam: A method for stochastic optimization, in: Proc. of the 3rd Int. Conf. for Learning Representations, San Diego, USA, 2015.

[27] D. Yu, M. L. Seltzer, Improved bottleneck features using pretrained deep neural networks, in: Twelfth Annual Conference of the International Speech Communication Association, 2011, pp. 237–240.

[28] M. Woodard, K. Marashi, S. Sedigh Sarvestani, A. R. Hurson, Survivability evaluation and importance analysis for cyber-physical smart grids, Rel. Eng. & Syst. Safety 210 (2021) 107479. doi:10.1016/j.ress.2021.107479.

[29] University of Washington, Power systems test case archive, http://www.ee.washington.edu/research/pstca/ (retrieved January 2021).

[30] M. Asprou, E. Kyriakides, Optimal PMU placement for improving hybrid state estimator accuracy, in: IEEE Trondheim PowerTech, 2011, pp. 1–7. doi:10.1109/PTC.2011.6019247.

[31] N. Acharya, N. Mithulananthan, Locating series FACTS devices for congestion management in deregulated electricity markets, Electric Power Systems Research 77 (3–4) (2007) 352–360. doi:10.1016/j.epsr.2006.03.016.

[32] K. Marashi, S. Sedigh Sarvestani, Towards comprehensive modeling of reliability for smart grids: Requirements and challenges, in: Proc. of the 15th IEEE Int. High Assurance Syst. Eng. Symposium (HASE '14), Miami, FL, 2014, pp. 105–112. doi:10.1109/HASE.2014.23.

[33] K. Marashi, S. Sedigh Sarvestani, A. R. Hurson, Consideration of cyber-physical interdependencies in reliability modeling of smart grids, IEEE Trans. Sustain. Comput. – Special Issue on Sustainable Cyber-Physical Systems 3 (2) (2018) 73–83.

[34] EN 50160, voltage characteristics of electricity supplied by public distribution systems, Tech. rep., CENELEC (2005).

[35] Y. Song, B. Wang, Survey on reliability of power electronic systems, IEEE Trans. Power Electron. 28 (1) (2013) 591–604. doi:10.1109/TPEL.2012.2192503.

[36] PowerWorld Corporation, http://www.powerworld.com/products/simulator/overview.

[37] DIgSILENT GmbH, http://www.digsilent.com/.

[38] MATPOWER, a MATLAB power system simulation package, http://www.pserc.cornell.edu/matpower/.

[39] F. Milano, An open source power system analysis toolbox, IEEE Trans. Power Syst. 20 (3) (2005) 1199–1206. doi:10.1109/TPWRS.2005.851911.

[40] M. Abadi, A. Agarwal, P. Barham, E. Brevdo, Z. Chen, C. Citro, G. S. Corrado, A. Davis, J. Dean, M. Devin, S. Ghemawat, I. J. Goodfellow, A. Harp, G. Irving, M. Isard, Y. Jia, R. Józefowicz, L. Kaiser, M. Kudlur, J. Levenberg, D. Mané, R. Monga, S. Moore, D. G. Murray, C. Olah, M. Schuster, J. Shlens, B. Steiner, I. Sutskever, K. Talwar, P. A. Tucker, V. Vanhoucke, V. Vasudevan, F. B. Viégas, O. Vinyals, P. Warden, M. Wattenberg, M. Wicke, Y. Yu, X. Zheng, TensorFlow: Large-scale machine learning on heterogeneous distributed systems (2015).
URL http://download.tensorflow.org/paper/whitepaper2015.pdf

Appendix A. Largest Dependency Links (d_{ij})

Table A.5: Notable dependencies among components of IEEE-14 smart grid.

PCC		**RDC**		**Causation**	
Components	d_{ij}	Components	d_{ij}	Components	d_{ij}
L_{1-2} - L_{1-5}	0.73	L_{1-2} - L_{1-5}	0.83	L_{1-2} - L_{1-5}	0.83
L_{2-3} - F_{2-3}	0.60	L_{2-3} - F_{2-3}	0.79	L_{2-3} - F_{2-3}	0.81
L_{2-4} - F_{2-4}	0.52	L_{2-4} - F_{2-4}	0.72	L_{2-4} - F_{2-4}	0.77
P_2 - L_{1-2}	0.49	L_{4-5} - L_{1-2}	0.61	L_{1-5} - F_{1-5}	0.56
F_{1-5} - L_{1-2}	0.48	P_2 - L_{1-2}	0.60	F_{1-5} - L_{1-2}	0.39
L_{4-5} - L_{1-2}	0.45	F_{1-5} - L_{1-2}	0.57	P_2 - L_{1-2}	0.32
L_{1-5} - F_{1-5}	0.43	L_{1-5} - F_{1-5}	0.56	L_{1-5} - P_9	0.20
F_{1-5} - L_{1-5}	0.35	F_{1-5} - L_{1-5}	0.52	L_{2-3} - L_{4-5}	0.13
L_{2-3} - L_{1-5}	0.34	L_{1-5} - L_{1-2}	0.46	DS - L_{1-2}	0.12
L_{4-9} - L_{1-2}	0.33	L_{2-3} - L_{1-5}	0.46	L_{7-9} - L_{9-10}	0.12

Table A.6: Notable dependencies among components of IEEE-57 smart grid.

PCC		**RDC**		**Causation**	
Components	d_{ij}	Components	d_{ij}	Components	d_{ij}
L_{1-17} - F_{1-17}	0.76	L_{7-29} - L_{8-9}	0.96	L_{12-17} - F_{12-17}	0.95
L_{7-29} - L_{8-9}	0.73	L_{12-17} - F_{12-17}	0.94	L_{1-17} - F_{1-17}	0.94
L_{12-17} - F_{12-17}	0.72	L_{1-17} - F_{1-17}	0.93	L_{28-29} - P_{28}	0.92
L_{2-3} - L_{1-15}	0.69	L_{28-29} - P_{28}	0.92	L_{7-29} - L_{8-9}	0.92
F_{1-16} - F_{1-16}	0.68	L_{34-35} - P_{32}	0.92	L_{1-16} - F_{1-16}	0.91
L_{7-8} - F_{7-8}	0.67	L_{9-55} - P_{53}	0.92	L_{37-38} - P_{56}	0.91
L_{34-35} - P_{32}	0.65	L_{37-38} - P_{32}	0.92	L_{7-8} - F_{7-8}	0.91
L_{28-29} - P_{28}	0.65	L_{37-38} - P_{56}	0.92	L_{6-7} - F_{6-7}	0.90
L_{9-55} - P_{53}	0.65	L_{34-32} - P_{32}	0.91	L_{54-55} - F_{54-55}	0.88
L_{37-38} - P_{32}	0.65	L_{35-36} - P_{32}	0.91	L_{7-29} - P_{28}	0.87

Appendix B. Largest Multi-step Dependency Links (t_{ij})

Table B.7: Notable multi-step dependency links among components of IEEE-14 smart grid; dependency links that are relatively large in **T**, but small in **D**.

PCC	**RDC**	**Causation**
Components	Components	Components
L_{2-3} - L_{1-2}	L_{2-3} - L_{1-2}	L_{1-2} - F_{1-5}
L_{4-5} - L_{1-5}	L_{2-3} - L_{1-5}	F_{1-5} - L_{1-5}
L_{2-3} - L_{1-5}	L_{4-5} - L_{1-5}	P_2 - L_{1-5}
L_{2-4} - L_{1-5}	L_{2-4} - L_{1-5}	L_{1-5} - L_{1-2}
L_{2-3} - F_{1-5}	L_{2-3} - F_{1-5}	L_{1-2} - P_9
L_{2-3} - L_{1-2}	L_{2-4} - L_{1-2}	P_2 - F_{1-5}
P_2 - L_{1-5}	L_{2-4} - F_{1-5}	DS - L_{1-5}
L_{2-4} - L_{1-2}	L_{4-5} - F_{1-5}	F_{1-5} - P_9
L_{2-4} - F_{1-5}	L_{5-6} - L_{1-5}	L_{4-5} - L_{1-5}
L_{5-6} - L_{1-5}	L_{7-9} - L_{1-5}	DS - F_{1-5}

Table B.8: Notable multi-step dependency links among components of IEEE-57 smart grid; dependency links that are relatively large in **T**, but small in **D**.

PCC	**RDC**	**Causation**
Components	Components	Components
L_{7-29} - L_{1-15}	L_{7-29} - L_{1-15}	L_{7-29} - L_{7-8}
L_{7-29} - L_{1-2}	L_{7-29} - L_{1-2}	L_{7-8} - F_{6-8}
L_{7-29} - F_{7-8}	L_{7-29} - F_{7-8}	L_{8-9} - F_{7-8}
L_{7-29} - P_{32}	L_{1-16} - P_{32}	L_{1-16} - L_{1-2}
L_{7-29} - F_{1-17}	L_{7-29} - F_{1-17}	L_{7-29} - L_{6-8}
L_{7-29} - L_{1-17}	L_{7-29} - L_{1-17}	L_{1-15} - F_{1-17}
L_{1-16} - P_{32}	L_{7-29} - P_{32}	L_{8-9} - F_{6-8}
L_{7-29} - L_{7-8}	L_{1-2} - P_{32}	L_{1-2} - F_{1-17}
L_{1-15} - P_{32}	L_{1-15} - P_{32}	P_{32} - F_{1-17}
L_{8-9} - L_{1-15}	L_{1-16} - F_{1-17}	L_{1-2} - F_{1-16}

Appendix C. Largest Out-degree Values (τ_i)

Table C.9: Weighted out-degree of components of the IEEE-14 smart grid.

PCC		**RDC**		**Causation**	
Component	τ	Components	τ	Component	τ
L_{2-3}	0.239	L_{2-3}	0.244	L_{1-2}	0.206
L_{4-5}	0.219	L_{4-5}	0.234	L_{1-5}	0.187
L_{2-4}	0.215	L_{2-4}	0.220	L_{4-5}	0.152
L_{1-2}	0.205	L_{1-2}	0.206	F_{1-5}	0.143
P_9	0.196	L_{7-9}	0.200	L_{2-3}	0.128
L_{1-5}	0.193	P_2	0.199	P_2	0.127
F_{1-5}	0.188	L_{5-6}	0.197	L_{2-4}	0.113
P_2	0.187	L_{1-5}	0.196	P_9	0.093
F_{2-3}	0.185	F_{1-5}	0.194	DS	0.091
L_{5-6}	0.178	P_9	0.191	L_{7-9}	0.071

Table C.10: Weighted out-degree of components of the IEEE-57 smart grid.

PCC		**RDC**		**Causation**	
Component	τ	Components	τ	Component	τ
L_{7-29}	0.073	L_{7-29}	0.072	L_{1-2}	0.047
L_{8-9}	0.069	L_{1-16}	0.067	L_{7-29}	0.038
L_{1-2}	0.063	L_{1-2}	0.067	L_{1-15}	0.033
L_{1-16}	0.063	L_{8-9}	0.067	L_{1-16}	0.031
L_{1-15}	0.062	L_{1-15}	0.063	L_{7-8}	0.028
L_{7-8}	0.055	L_{3-4}	0.060	L_{22-23}	0.025
P_{25}	0.053	L_{22-23}	0.060	L_{8-9}	0.024
L_{12-17}	0.052	L_{37-39}	0.058	L_{1-17}	0.018
P_{19}	0.051	L_{7-8}	0.056	L_{37-38}	0.018
P_{28}	0.050	L_{12-17}	0.054	L_{6-8}	0.016

Appendix D. Largest In-degree Values (ν_j)

Table D.11: Weighted in-degree of components of the IEEE-14 smart grid.

PCC		**RDC**		**Causation**	
Component	ν	Components	ν	Component	ν
L_{1-2}	0.591	L_{1-5}	0.604	L_{1-5}	0.181
L_{1-5}	0.575	L_{1-2}	0.594	L_{1-2}	0.1168
F_{1-5}	0.497	F_{1-5}	0.495	F_{1-5}	0.151
P_9	0.421	P_9	0.427	P_9	0.148
F_{2-3}	0.318	F_{2-3}	0.322	L_{4-5}	0.118
F_{2-4}	0.269	L_{4-5}	0.285	L_{9-10}	0.103
L_{4-5}	0.263	F_{2-4}	0.280	F_{2-3}	0.101
L_{2-3}	0.219	L_{9-10}	0.237	L_{7-9}	0.093
L_{9-10}	0.187	L_{2-3}	0.210	F_{2-4}	0.088
L_{7-9}	0.175	L_{7-9}	0.208	L_{2-3}	0.080

Table D.12: Weighted in-degree of components of the IEEE-57 smart grid.

PCC		**RDC**		**Causation**	
Component	ν	Components	ν	Component	ν
F_{1-17}	0.130	L_{1-17}	0.132	P_{32}	0.045
L_{1-17}	0.130	F_{1-17}	0.128	L_{1-17}	0.043
P_{32}	0.116	P_{32}	0.126	F_{1-17}	0.031
L_{1-15}	0.101	L_{1-15}	0.109	L_{1-15}	0.028
L_{1-2}	0.086	L_{1-2}	0.099	P_{28}	0.027
P_{28}	0.083	P_{25}	0.092	P_{53}	0.023
P_{25}	0.081	P_{28}	0.092	L_{8-9}	0.022
P_{53}	0.081	P_{53}	0.089	P_{25}	0.020
F_{1-16}	0.077	F_{1-16}	0.084	L_{7-8}	0.019
F_{7-8}	0.077	P_{56}	0.084	P_{56}	0.019